



HAL
open science

The tomato P69 subtilase family is involved in resistance to bacterial wilt

Weiqi Zhang, Marc Planas-Marquès, Marianne Mazier, Margarita Šimkovicová, Mercedes Rocafort, Melissa Mantz, Pitter Huesgen, Frank Takken, Annick Stintzi, Andreas Schaller, et al.

► To cite this version:

Weiqi Zhang, Marc Planas-Marquès, Marianne Mazier, Margarita Šimkovicová, Mercedes Rocafort, et al.. The tomato P69 subtilase family is involved in resistance to bacterial wilt. *Plant Journal*, 2023, 10.1111/tpj.16613 . hal-04398628

HAL Id: hal-04398628

<https://hal.science/hal-04398628>

Submitted on 7 Mar 2024



HAL is a multi-disciplinary open access archive for the deposit and dissemination of scientific research documents, whether they are published or not. The documents may come from teaching and research institutions in France or abroad, or from public or private research centers.

L'archive ouverte pluridisciplinaire **HAL**, est destinée au dépôt et à la diffusion de documents scientifiques de niveau recherche, publiés ou non, émanant des établissements d'enseignement et de recherche français ou étrangers, des laboratoires publics ou privés.



Distributed under a Creative Commons Attribution - NonCommercial 4.0 International License

The tomato P69 subtilase family is involved in resistance to bacterial wilt

WeiQi Zhang^{1,†}, Marc Planas-Marqués^{1,2,†}, Marianne Mazier³, Margarita Šimkovicová⁴, Mercedes Rocafort¹, Melissa Mantz^{5,6}, Pitter F. Huesgen^{5,6,7}, Frank L. W. Takken⁴ , Annick Stintzi⁸, Andreas Schaller⁸, Nuria S. Coll^{1,9,*}  and Marc Valls^{1,2,*}

¹Centre for Research in Agricultural Genomics (CRAG), CSIC-IRTA-UAB-UB, Campus UAB, Bellaterra, Spain,

²Department of Genetics, Microbiology and Statistics, Universitat de Barcelona, Barcelona, Catalonia, Spain,

³GAFI UR 1052, INRAE, Montfavet F84143, France,

⁴Molecular Plant Pathology, Faculty of Science, Swammerdam Institute for Life Sciences, University of Amsterdam, Amsterdam, The Netherlands,

⁵Central Institute for Engineering, Electronics and Analytics, ZEA-3, Forschungszentrum Jülich, Jülich, Germany,

⁶CECAD, Medical Faculty and University Hospital, University of Cologne, Cologne, Germany,

⁷Faculty of Mathematics and Natural Sciences, Institute for Biochemistry, University of Cologne, Cologne, Germany,

⁸Department of Plant Physiology and Biochemistry, University of Hohenheim, Stuttgart, Germany, and

⁹Consejo Superior de Investigaciones Científicas (CSIC), Barcelona, Spain

Received 1 September 2023; revised 13 December 2023; accepted 15 December 2023.

*For correspondence (e-mail marcvalls@ub.edu; nuria.sanchez-coll@cragenomica.es).

[†]These authors contributed equally to the work.

SUMMARY

The intercellular space or apoplast constitutes the main interface in plant–pathogen interactions. Apoplastic subtilisin-like proteases—subtilases—may play an important role in defence and they have been identified as targets of pathogen-secreted effector proteins. Here, we characterise the role of the Solanaceae-specific P69 subtilase family in the interaction between tomato and the vascular bacterial wilt pathogen *Ralstonia solanacearum*. *R. solanacearum* infection post-translationally activated several tomato P69s. Among them, P69D was exclusively activated in tomato plants resistant to *R. solanacearum*. *In vitro* experiments showed that P69D activation by prodomain removal occurred in an autocatalytic and intramolecular reaction that does not rely on the residue upstream of the processing site. Importantly P69D-deficient tomato plants were more susceptible to bacterial wilt and transient expression of *P69B*, *D* and *G* in *Nicotiana benthamiana* limited proliferation of *R. solanacearum*. Our study demonstrates that P69s have conserved features but diverse functions in tomato and that P69D is involved in resistance to *R. solanacearum* but not to other vascular pathogens like *Fusarium oxysporum*.

Keywords: apoplast, plant defence, *Ralstonia solanacearum*, serine protease, *Solanum lycopersicum*.

INTRODUCTION

The extracellular space or apoplast plays a key role in plant–pathogen interactions. Both plants and pathogens secrete proteases, protease inhibitors, glycoside hydrolases, peroxidases and antioxidant enzymes into this compartment (Du et al., 2016). Plant pattern recognition receptors recognise microbe- and danger-associated molecular patterns in the apoplast and activate immune responses (Macho & Zipfel, 2014). However, due to the ease of collecting the leaf apoplastic fluid (Gupta et al., 2015), most of these studies have been limited to foliar pathogens and the role of apoplastic enzymes in the interaction with vascular pathogens is largely unexplored.

Two families of proteases are of particular interest with respect to their role in plant defence: the papain-like cysteine proteases (PLCPs), and the subtilisin-like proteases (subtilases). Subtilases are serine proteases present in all living organisms and involved in various processes, from embryogenesis to senescence (Schaller et al., 2018). Subtilases possess an aspartate, histidine, serine catalytic triad (Smith et al., 1966) and are synthesised as pre-pro-enzymes with an N-terminal signal peptide and an autoinhibitory prodomain that needs to be cleaved for secretion and activation of the protease (Meyer et al., 2016; Schaller et al., 2018). This prodomain processing is an intramolecular (autocatalytic) processing event (Cedzich et al., 2009;

Meyer et al., 2016; Nebes & Jones, 1991; Power et al., 1986; Vey et al., 1994) and depends on the active site serine (Cedzich et al., 2009; Chichkova et al., 2010). Thus, the amino acid sequence at the cleavage site is expected to reflect the substrate specificity of the protease (Muller et al., 2000). This is observed for the aspartate-specific phytaspases, which feature an aspartic acid residue upstream of the cleavage site (Chichkova et al., 2010; Reichardt et al., 2018), while in other plant subtilases, the TTXS/T motif at the N-terminus of the mature protease appears to be more relevant for cleavage site recognition (Meyer et al., 2016). The mature sequence of subtilases contains a subtilase catalytic domain, a protease-associated domain and a fibronectin III-like domain (Schaller et al., 2018). The protease-associated domain has been implicated in protein–protein interactions (Mahon & Bateman, 2000) and substrate binding specificity (Schaller et al., 2018; Tan-Wilson et al., 2012), while the fibronectin III-like domain appears to confer stability to the enzyme (Ottmann et al., 2009).

Tomato P69A, initially named pathogenesis-related protein 7 (PR-7), is the first subtilase for which a role in plant defence was reported (Vera & Conejero, 1988, 1989). The protein localises in the extracellular space and occasionally inside the vacuole (Vera et al., 1989). Subsequent studies identified a total of six P69 genes in tomato, which were named *P69A* to *F* (Jorda et al., 1999, 2000; Meichtry et al., 1999). *P69B* and *P69C*, are systemically induced by *Pseudomonas syringae* infection and salicylic acid treatment (Jorda et al., 2000; Meichtry et al., 1999). Of note, *P69C* cleaves a leucin-rich repeat protein located in the extracellular matrix, which was speculated to trigger immune signalling (Tornero et al., 1996). Recently, other P69 genes were shown to be upregulated upon infection with various pathogens, including *Phytophthora infestans* (Tian et al., 2004) and *Ralstonia solanacearum* (Ishihara et al., 2012; Zuluaga et al., 2015). *P69B* was recently found to cleave the small cysteine-rich secreted protein PC2 secreted from the potato late blight pathogen *P. infestans*, to trigger plant defence (Wang et al., 2021). *P69B* was also reported to participate in the maturation-by-cleavage of the Rcr3 protease (Paulus et al., 2020), thereby constituting the first proteolytic cascade identified in plants. Of note, Rcr3 and Pip1 papain-like cysteine proteases are inhibited by *Cladosporium fulvum* Avr2 effector and *P. infestans* EPIC1 and EPIC2B (Song et al., 2009; Tian et al., 2007). In addition, *P. infestans* secretes the Kazal-like protease inhibitors EPI1 and EPI10 that were shown to bind and inhibit *P69B* (Gupta et al., 2015; Paulus et al., 2020; Tian et al., 2004, 2005). The recent identification of *P69B* inhibitors in *Cladosporium fulvum*, *Fusarium oxysporum* and *Xanthomonas perforans* suggests that inactivation of *P69B* may be a general virulence strategy of diverse microbial pathogens (Homma et al., 2023).

Ralstonia solanacearum (some strains are also called *R. pseudosolanacearum*) is a bacterial vascular pathogen that causes wilt disease in over 200 plant species, including economically important crops such as tomato, potato, banana and pepper (Hayward, 1991). This soil-borne pathogen infects plants through the roots and eventually colonises the xylem, where it clogs infected vessels, causing plant wilting (Vasse et al., 1995). Before reaching the xylem, *R. solanacearum* multiplies in the intercellular spaces of the roots (Grimault et al., 1994).

We previously demonstrated that resistant tomato plants limit early root colonisation by *R. solanacearum* (Planas-Marques et al., 2020). As a first step to dissect the underlying mechanisms, we analysed the apoplast proteome upon challenge with *R. solanacearum* strain GMI1000 in susceptible (Marmande) and resistant (Hawaii 7996) tomato cultivars (Planas-Marques et al., 2018). Among all papain-like cysteine proteases and serine hydrolases, two closely related subtilases (P69D and P69J) were the most highly activated after infection. More recently, we identified a total of 10 P69 subtilases in the tomato genome (Reichardt et al., 2018). Here, we study the P69s most highly induced upon infection and we demonstrate that they have conserved features but diverse functions in tomato. We further show that P69D is involved in resistance to *R. solanacearum* but not to other vascular pathogens like *F. oxysporum*.

RESULTS

P69s are conserved subtilases present only in the nightshade family and activated in tomato upon *R. solanacearum* infection

Ten genes encoding P69 proteases have been annotated in the tomato genome (Reichardt et al., 2018) (Table S1). These cluster in a single 60 Kb region on chromosome 8, without any interspaced genes (Figure 1a). A neighbour-joining tree of the encoded amino acid sequences, including the closest non-P69 tomato subtilase (Solyc08g007680) as an outgroup, revealed that the most divergent proteins (P69E and F) occupy a distal position at one end of the genomic cluster (Figure 1b). The encoded proteins share a high percentage of identity (>82%). Comparison with other subtilisin-like proteases showed that they all possess the same conserved domains (Figure 1c) including a predicted N-terminal signal peptide and autoinhibitory prodomain, the subtilase domain with the conserved catalytic triad, the protease-associated domain (Mahon & Bateman, 2000) and the fibronectin-3-like domain (Cedzich et al., 2009) (Figure 1c). Although the N-terminal THT sequence motif of mature subtilases (Reichardt et al., 2018) was conserved, both the amino acid preceding the cleavage site and the specificity-conferring residue in the S1 binding pocket of the enzyme (Vartapetian et al., 2011) differed among P69s (Table S1).

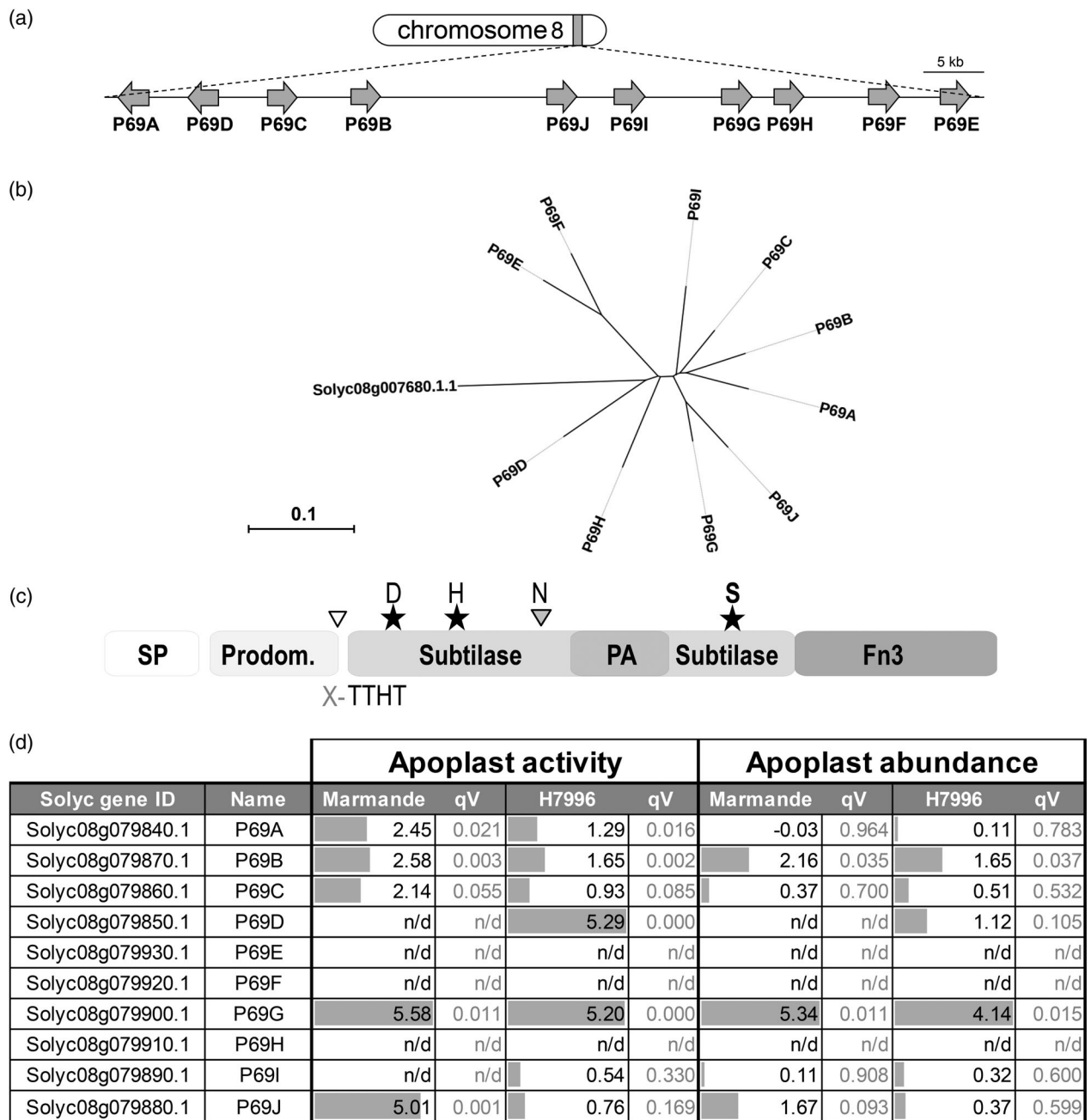


Figure 1. Genomic and protein features of the tomato P69 subtilases.

(a) Schematic representation of the genomic locus of tomato P69 subtilases.

(b) Neighbour-joining protein similarity tree of tomato P69 subtilases generated from a ClustalO alignment. The most highly related non-P69 tomato subtilase Solyc08g007680 was added as an outgroup. Scale bar indicates 0.1 changes per site per 100 nucleotides.

(c) Representation of the tomato P69 protein domains and conserved features. The predicted prodomain cleavage site marked by a white triangle. The position of the catalytic triad (D, H, S, asterisks), the conserved THTT motif and the putative oxyanion hole residue (N) (grey triangle) are indicated. Fn3, fibronectin III-like domain; PA, protease-associated domain; Prodom., prodomain; SP, signal peptide.

(d) Differential activation or accumulation of P69 subtilases in the apoplastic fluid. Log₂ FC of abundance for the active proteins ('Apoplast activity' and general protein abundance 'Apoplast abundance') in *Ralstonia solanacearum*-inoculated versus non-inoculated samples in susceptible (Marmande) and resistant (Hawaii 7996) tomato apoplast is shown for all P69s. Grey bars inside each cell are proportional to log₂ FC values. The *q*-value (qV) statistic is also indicated. n/d, not detected.

BLASTp searches identified orthologues in potato, eggplant, pepper, *Nicotiana tabacum* and *N. attenuata* with 91.8 to 83.1% sequence identity to P69D, while in non-solanaceous

genomes the closest proteins shared less than 68% sequence identity. *S. pimpinellifolium* P69D orthologues were found to be identical to those of tomato. All *bona fide*

P69s were identified in each species as candidate orthologues that clustered with tomato P69 sequences in neighbour-joining trees (Figure S1). P69A and P69D are conserved in all analysed species of the nightshade family. P69B, P69C, P69E and P69I were only found in tomato and potato, whereas P69G, P69H, P69J and P69F are unique in tomato (Figure S2).

To analyse changes in activity and abundance of P69 proteins in tomato in response to *R. solanacearum*, we re-analysed our activity-based proteome profiling dataset (Planas-Marques et al., 2018) where a biotinylated active site probe was used to pull down active serine hydrolases and to quantify their abundance in the tomato apoplast. We found that the activity of seven P69s increased in response to the pathogen in the resistant variety Hawaii 7996 while five proteases were also activated in susceptible plants (Figure 1d). P69D, G and J showed the highest increase in activity, while P69D was uniquely activated in the resistant cultivar (Figure 1d).

Cleavage specificity of *R. solanacearum*-induced P69 proteases

To investigate the activity and substrate specificity of tomato P69 subtilases, C-terminally His-tagged recombinant proteins were purified from apoplastic fluid after transient expression in *N. benthamiana* (Figure 2a; Figure S3). We confined our study to the members clearly activated in the apoplast upon *R. solanacearum* infection: P69A, P69B, P69C, P69D, P69G and P69J (Figure 1d). The activity of the purified proteins at neutral pH was measured using two fluorogenic substrates, a synthetic 11-mer peptide and casein. All enzymes effectively cleaved both substrates but P69A, P69C and P69D showed preference for the synthetic peptide while P69B, P69G and P69J were more active on casein (Figure 2b). The protease activity was measured for each protein over a range of pH using the preferred substrates. P69B, C and D were most active at neutral pH, while P69A, G and J also remained fully active at alkaline conditions (Figure 2c).

Next, we investigated substrate specificity of the selected P69s using the PICS (Proteomics Identification of Cleavage Sites) approach (Schilling et al., 2011; Schilling & Overall, 2008). Overall, all proteins exhibited similar selectivity for the five amino acids upstream of the scissile bond, where cleavage occurs (Figure 3). However, some particularities were observed. Firstly, P69A and P69B were the only P69s with a preference for aspartate in the P1 position (the position immediately upstream of the scissile bond). Secondly, P69D showed clear selectivity for the hydrophobic aliphatic residues isoleucine and valine in P2, while other P69s preferred proline in this position (Figure 3). All P69s showed a preference for hydrophobic aliphatic residues (isoleucine, leucine and/or valine) in P4, which was most pronounced for P69A and P69B. Overall,

P69s showed similar cleavage site selectivity and considerable cleavage promiscuity, suggesting that additional mechanisms may contribute to cleavage specificity *in vivo*.

P69B, P69D and P69G inhibit *R. solanacearum* growth

To investigate whether the P69s induced by *R. solanacearum* play a role in plant defence, we inoculated the pathogen in *N. benthamiana* leaves overexpressing the proteases and recorded bacterial growth over time. An *R. solanacearum* strain that is pathogenic on *N. benthamiana* was used for these experiments (GMI1000 devoid of the effectors AvrA and PopP2) (Poueymiro et al., 2009). Bacterial growth was impaired in leaves overexpressing P69B, C, D and G but not P69A or J, when compared to the empty vector control (Figure 4) 3 days post-inoculation (dpi). At this time point leaves showed no disease symptoms yet. The strongest effect was seen for P69D, which is the one most highly and specifically activated by pathogens in resistant plants (Figure 1d). Thus, we concentrated on this protein for further characterisation.

Characterisation of P69D self-processing, secretion and glycosylation

To investigate the requirements for prodomain self-removal in P69D, we generated a mutant replacing the putative catalytic serine and the histidine preceding TTHT by alanine (S532A and H114A, respectively). Contrary to WT P69D, the S532A mutant was not secreted into the apoplast (Figure 5a) upon transient expression in *N. benthamiana* and was retained in the cells in its unprocessed form (Figure 5b), indicating that this serine was required for enzyme maturation and secretion. Moreover, co-expression of WT P69D and S532A showed that prodomain removal occurred in an autocatalytic and intramolecular reaction since the mutant proteins could not be processed *in trans* by WT P69D (Figure 5a,b, *rightmost lanes*). The function of the signal peptide would thus be to ensure proper secretion to the apoplast and the presence of the mature protein only in this compartment. On the contrary, the H114A variant was processed and secreted into the apoplast, yet less efficiently than WT P69D (Figure 5a). This indicated that, unlike tobacco phytophage, prodomain cleavage in P69D does not rely on the residue upstream of the processing site, which is consistent with our PICS analysis showing that histidine is tolerated but not preferred in P1 (Figure 3).

Secreted P69s transiently expressed in *N. benthamiana*, showed bigger and varying sizes in SDS-PAGE likely due to post-translational modifications (Figure 2a). We therefore analysed if *N*-glycosylation could explain these apparent size differences. We predicted five putative *N*-glycosylation sites in P69D, four of which were previously confirmed experimentally for P69B (Bykova et al., 2006) (Figure S4a). Next, we estimated P69D molecular weight assuming that all putative sites were glycosylated either with

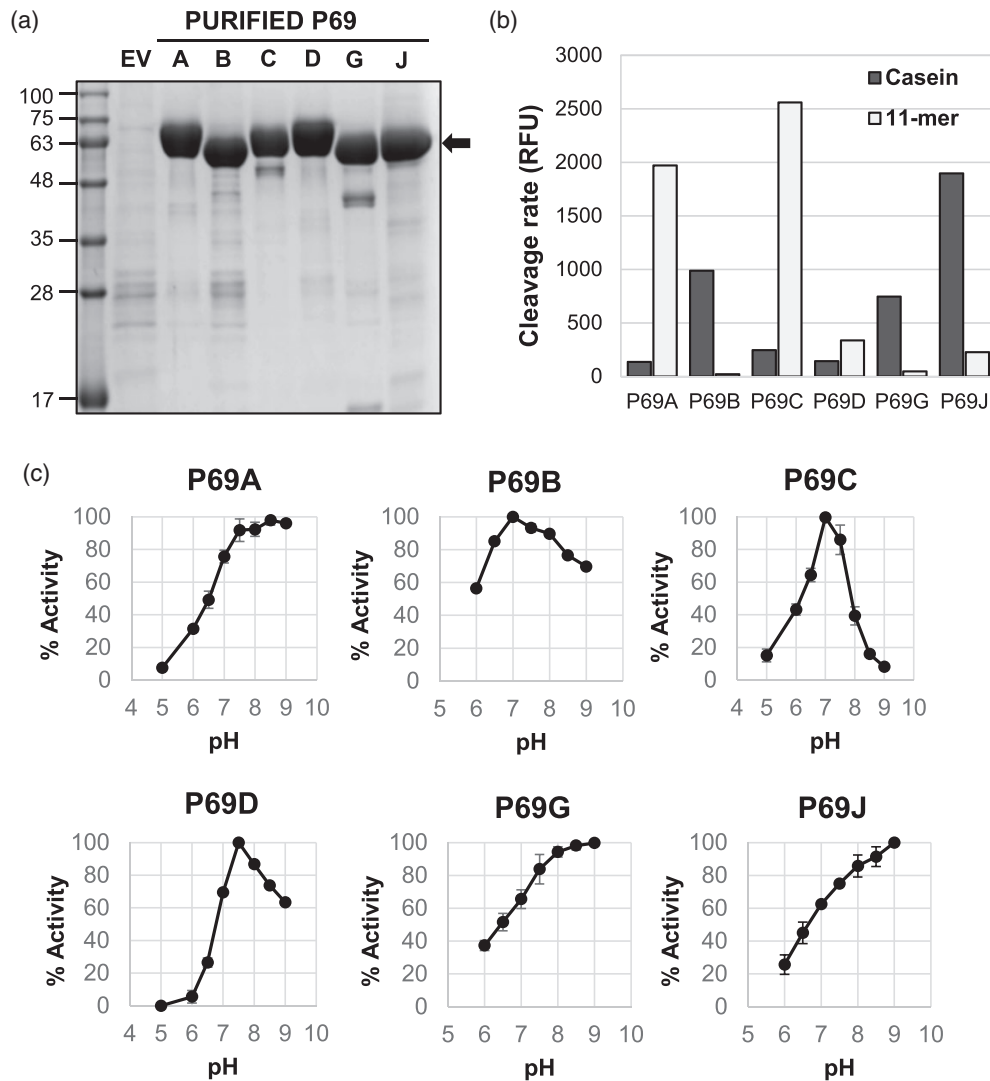


Figure 2. Enzymatic activity of recombinant tomato P69 subtilases.

(a) SDS-PAGE separation of purified P69 proteins (arrow) stained with Coomassie Brilliant Blue. The coding sequence of representative tomato P69s was fused to a C-terminal hexa-His-tag and transiently expressed in *Nicotiana benthamiana* leaves. Proteins were purified by metal chelate affinity chromatography from apoplastic fluid harvested 5 days after agroinfiltration. A mock-purified fraction from empty vector infiltrated plants is shown as control (EV).

(b) Activity assay of recombinant P69s at pH 7 using a synthetic 11-mer peptide or casein as substrates. RFU, relative fluorescent units.

(c) P69 activity at different pH. Activity in a three-component buffer system using the 11-mer peptide (P69A, P69C, P69D) or casein (P69B, P69G, P69J) as fluorogenic substrates is shown as percentage of maximum activity at optimal pH. Average values of two technical replicates from two independent enzyme purifications ($n = 4$) are shown. Error bars indicate standard deviation.

the lighter, the most abundant or the heaviest glycans identified in P69B (Figure S4b). Since these estimated weights were still 7–20 kDa smaller than those observed in the SDS-PAGE (Figure S4b), we suggest that P69D may be subject to additional post-translational modifications or larger glycans that account for the observed mass differences.

Identification of candidate P69D substrates using proteomics and N-terminomics

To determine putative tomato P69D protein substrates, P69D-deficient tomato plants were generated using

CRISPR/Cas9 technology (Danilo et al., 2018) (Figure S5). Cas9-free homozygous mutants were obtained in the resistant tomato cv Hawaii 7996. Two sibling lines that carried a 202 bp deletion (P69D^{Δ202}) giving rise to a truncated P69D protein lacking the catalytic site serine were selected for analysis (Figure S5b). These lines showed a small but significant decrease in fresh weight when compared to the H7996 WT plants (Figure S7b).

We next isolated apoplastic proteomes from WT and P69D-deficient plants after infection with *R. solanacearum*. Quantitative apoplast proteome comparison identified 530

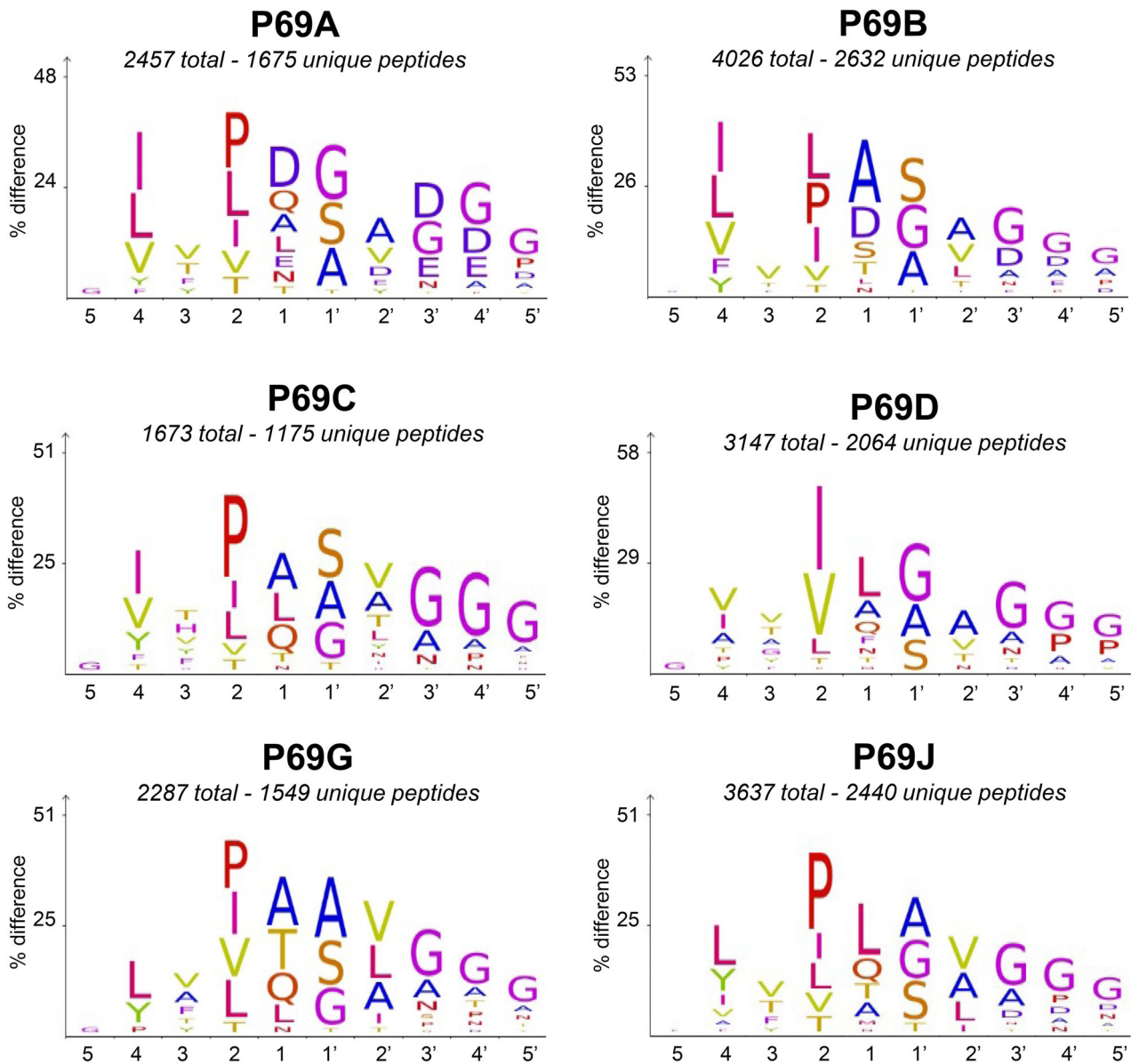


Figure 3. Substrate cleavage specificity of tomato P69s analysed by PICS.

IcelLogo graphs showing the amino acids observed upstream (positions 1 to 5) and downstream (positions 1' to 5') of the scissile bond. Letter size reflects the relative frequency of an amino acid at a given position as compared to natural abundance in the tomato proteome. Only residues that are significantly different from natural abundance at $P < 0.05$ are shown. The number of total and unique peptides identified by mass spectrometry is indicated in each panel. PICS, Proteomics Identification of Cleavage Sites.

proteins that were quantified in at least two of the three independent replicates (Data S1). Of these, nine proteins were significantly over-represented in WT ($\pi > 1.1082$), most prominently P69D itself (Figure 6a). Sixteen proteins were more abundant in the knockout apoplast ($\pi < -1.1082$), including several defence-related proteins such as PR1b, an osmotin-like protein, an aspartic protease of the A1 family and a carboxypeptidase (Figure 6a). HUNTER N-terminome analysis (Demir et al., 2022) further identified 419 N-terminal peptides from 249 proteins that were quantified in two of three replicates (Data S2), of which 50

showed significantly different accumulation (Figure 6b). Nineteen of the N-terminal peptides accumulating in WT and 22 of the N-terminal peptides more abundant in the P69D knockout mutant arose from proteolytic processing *in vivo*, as their newly generated N-termini were dimethylated (modified during the enrichment procedure) and matched to positions within the protein sequences. Strikingly, 19 N-terminal peptides came from the pathogenesis-related protein 1B (PR-1B), of which three were more abundant in wild type while five were more prevalent in the absence of P69D. Also, three peptides derived from

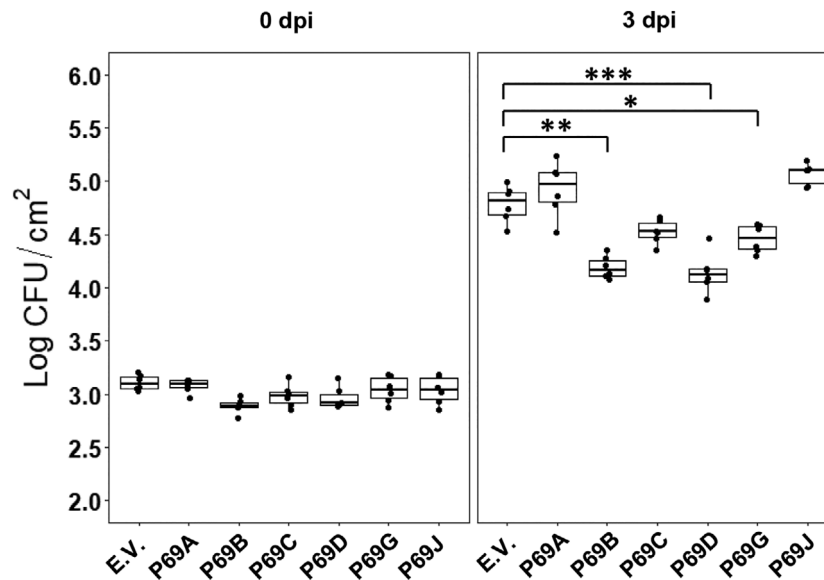


Figure 4. Phenotypes caused by overexpression of P69s.

Multiplication of *Ralstonia solanacearum* in *Nicotiana benthamiana* leaves transiently overexpressing P69s. *Agrobacterium* C58C1 harbouring plasmid pART27 (EV) or the same plasmid including P69s expression constructs were infiltrated into *N. benthamiana* leaves and 2 days later, inoculated by infiltration with 10^5 CFU ml⁻¹ of a virulent *R. solanacearum* strain defective in the avirulence genes *avrA* and *popP1*. Bacterial multiplication in leaves was assessed at 2 days post-inoculation (dpi). Each dot corresponds to a biological replica of an independent leaf. Significant differences to the empty vector are shown as, * $P < 0.05$, ** $P < 0.01$ and *** $P < 0.001$ (Student's *t*-test, $n = 6$).

cleaved PR2, which accumulated in the wild type, but not in the mutant (Figure 6b). This suggested that P69D may be involved in the processing of PR1B and PR2. In addition, we also observed a variety of differentially processed N-terminal peptides arising from P69 proteases and other subtilases (Data S2).

To identify direct P69D-mediated cleavages, we isolated apoplastic proteomes under non-denaturing conditions from P69D-deficient plants after infection with *R. solanacearum* and incubated this apoplast proteome *in vitro* with recombinant P69D or a control obtained using the same vector without cloned genes subject to the same extraction and purification procedure. Subsequent HUNTER N-terminome analysis determined 459 N-terminal peptides that were quantified in two of four replicates, of which 38 derived from PR-proteins (Figure S6a; Data S3). To our surprise, only three putative cleavage products (dimethylated N-terminal peptides) moderately increased (LIMMA-moderated *t*-test P -value < 0.05 and $\log_2 > 1$) after incubation with P69D and all were from proteins that appeared as likely contaminants. In contrast, 10 N-terminal peptides, including six termini derived from PR proteins cleavage (four from PR1B and two from PR2), showed significantly lower abundance, suggesting that other proteases are responsible for initial processing and that the cleavage products are then further degraded by P69D.

To verify that the added recombinant P69D was active and could cleave intact protein substrates, we additionally extracted total proteomes under non-denaturing conditions

from leaves of *R. solanacearum*-infected P69D-deficient mutant plants and incubated them with recombinant P69D. HUNTER N-terminome analysis identified 617 N-terminal peptides that were quantified in two or three replicates (Data S4), of which 134 matching to internal positions corresponding protein sequences accumulated significantly (LIMMA-moderated *t*-test P -value < 0.05 and $\log_2 > 1$), thus representing likely 69D cleavage sites (Figure S6b). Icelogo analysis of these P69D-generated cleavage sites showed strong agreement with the sequence logos derived from the peptide-based PICS analysis with Ile and Val preferred at P2 and small amino acids at P1', demonstrating that P69D can cleave intact proteins that present this motif (Figure S6c). However, none of these identified cleavage sites came from proteins with known apoplastic location.

Taken together, apoplast proteome and N-terminome analyses suggest that P69D-deficiency results in altered proteolytic processing of pathogenesis-related proteins, particularly PR1B and PR2 in the apoplast *in vivo* (Figure 6). However, this is likely not a direct effect as incubation of apoplast proteomes with recombinant P69D resulted in the degradation of some of the differentially cut PR1B protein termini, but not generation of new termini (Figure S6c).

Deletion of P69D in resistant tomato cv Hawaii 7996 compromises its resistance to *R. solanacearum*

To determine the functional relevance of P69D in the tomato–*R. solanacearum* interaction, we inoculated wild-type and P69D-deficient tomato lines with *R. solanacearum*

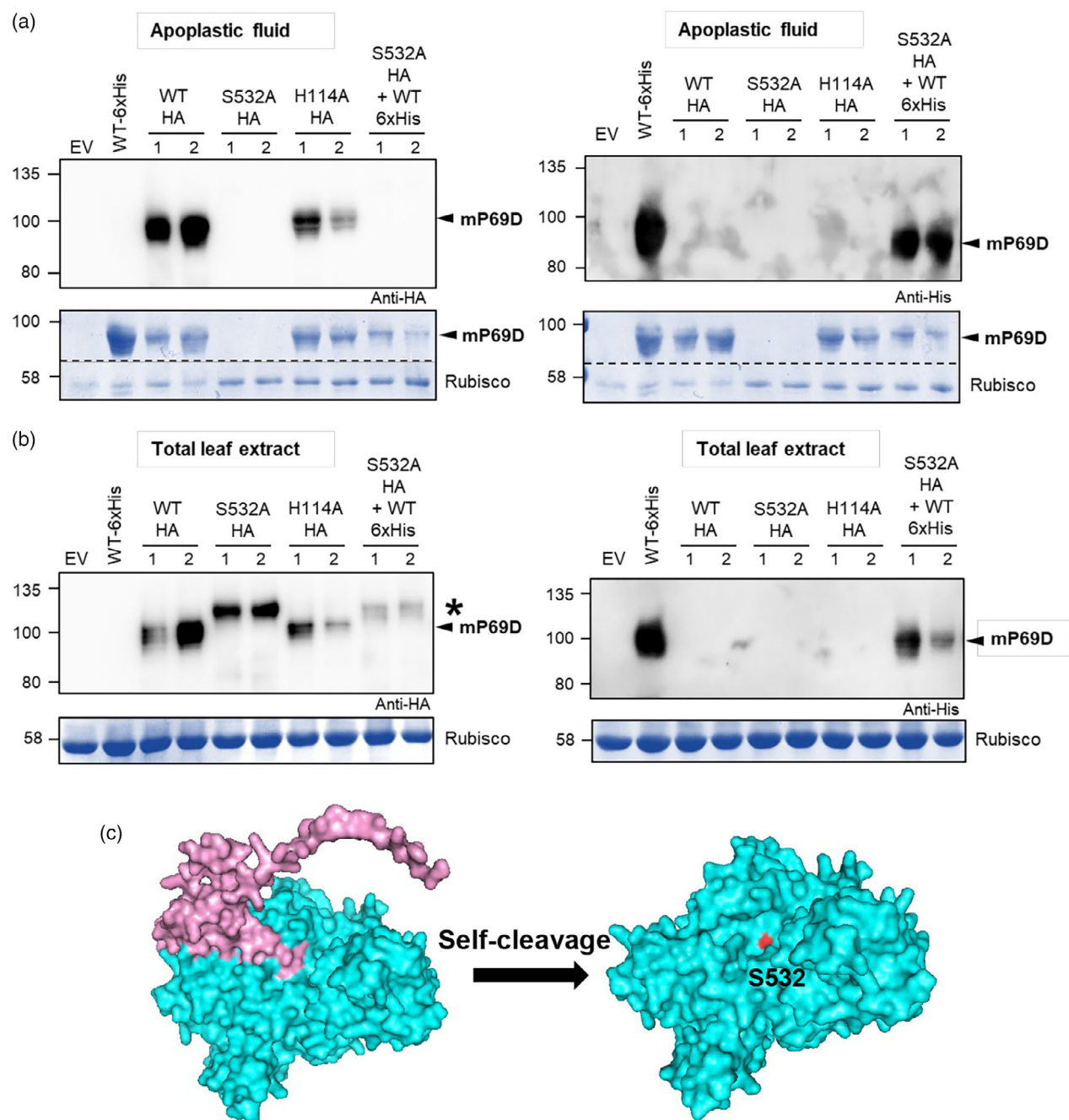


Figure 5. Serine-532 is required for P69D self-processing and secretion. Hexahistidine- (6xH) or hemagglutinin- (HA) tagged wild type (WT) P69D and its mutant variants S532A and H114A were transiently expressed in *Nicotiana benthamiana* leaves.

Apoplastic fluids (a) and total leaf extracts (b) were sampled 5 days after agroinfiltration and blotted using either α -His-tag or α -HA antibodies. The results of two biological replicates using different transformed *Agrobacterium* clones were used. Arrowheads and asterisk indicate the position of mature (mP69D) and immature P69D, respectively. An empty vector (EV) control was included. Bottom loading panels correspond to SDS-PAGE of the same samples stained with Coomassie brilliant blue.

(c) Modelled structures of tomato P69D full length (left) and its prodomain-less mature form using AlphaFold2. Signal peptide and prodomain are coloured in pink, the mature P69D protein in cyan and the catalytic site serine 532 in red.

by soil drenching. Mutant lines were more susceptible than the Hawaii 7996 wild type, although not as susceptible as cv Marmande (Figure 7A,B). Quantification of *R. solanacearum* concentrations in the roots or the base of the

hypocotyl 5 dpi revealed that hypocotyls of P69D-deficient Hawaii 7996 plants contained three to four times more bacteria than the resistant WT, but clearly less than the susceptible cv Marmande. On the contrary, no differences in

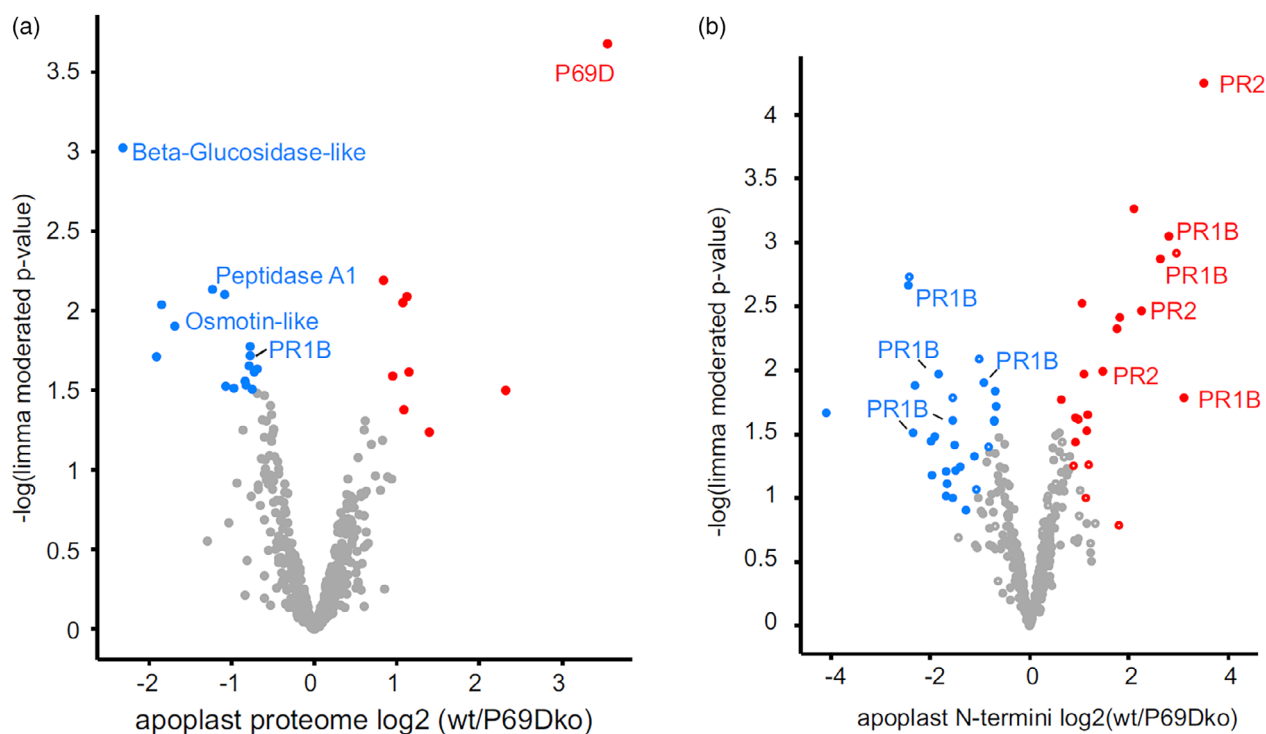


Figure 6. P69D proteome and N-terminome analyses.

(a) Volcano plot depicting changes in the apoplast leaf proteome of P69D-deficient plants compared to wild type, both infected with *Ralstonia solanacearum*. Red and blue, proteins significantly accumulating ($\pi > 1.1082$) and depleted ($\pi < -1.1082$), respectively, in wild type compared to P69D-deficient plants.

(b) N-terminome analysis of the same samples as in (a). Open circles, N-termini mapping to canonical protein termini (position 1 or 2 with intact or removed Met, known signal- or transit peptide sequences); filled circles, non-canonical protein termini mapping to positions within their protein sequence; red and blue, N-terminal peptides significantly accumulating or depleted ($\pi > 1.1082$ or $\pi < -1.1082$ respectively) after addition of P69D.

bacterial loads could be observed in the roots of the WT and the P69D mutant lines (Figure 7C). Interestingly, when the pathogen was inoculated directly into the stem, no significant wilting differences between the P69-deficient plants and wild-type H7996 were observed (Figure S7).

To check the specificity of the P69D-mediated disease resistance, we inoculated WT and P69D mutant plants with the vascular fungal pathogen *F. oxysporum* f.sp. *lycopersici* (Fol) and the bacterial leaf pathogen *P. syringae* pv. tomato (*Pst*). Analyses of the disease index and fresh weight revealed that the absence of functional P69D did not affect resistance to Fol (Figure S8). Additionally, bacterial load analysis on leaves demonstrated that resistance to *Pst* was also unaffected (Figure S8). Thus, P69D is important for tomato resistance against bacterial wilt but not against other vascular or foliar pathogens.

DISCUSSION

Conservation and function of P69 subtilase sequence identity and substrate specificity

Since the discovery of the first P69 family member as a protein induced by the Citrus Exocortis Viroid (Granell et al., 1987), these proteins have been implicated in all sorts

of plant-pathogen interactions, including bacteria, fungi and oomycete infections (French et al., 2018; Gawehns et al., 2015; Ishihara et al., 2012; Jorda et al., 1999; Planas-Marques et al., 2018; Tian et al., 2004, 2005; Tornero et al., 1997; Zuluaga et al., 2016). P69B and P69G are the two members most responsive to pathogens, being highly accumulated during *R. solanacearum* infection (Figure 1d). P69 B, C and G are also induced by the vascular pathogen *F. oxysporum* (de Lamo et al., 2018; Gawehns et al., 2015). Although potential substrates of P69s have been proposed during the last 30 years, including RuBisCO for P69A (Vera & Conejero, 1988) and a leucine-rich repeat protein for P69C (Tornero et al., 1996), their function in immunity has remained elusive. Recently, the secreted tomato PLCP Rcr3 has been reported as a substrate of P69B (Paulus et al., 2020). Rcr3 involved both in basal and gene-for-gene resistance against various pathogens, is also targeted by a distantly related subtilase, suggesting that redundant protease activities are required to ensure robust Rcr3-dependent immune responses (Paulus et al., 2020). Other P69s, such as P69A that also show a preference for aspartate in position P1 (Reichardt et al., 2018), could also participate in this process.

Interrogation of our activity-based protease profiling data highlighted several P69 family members as good

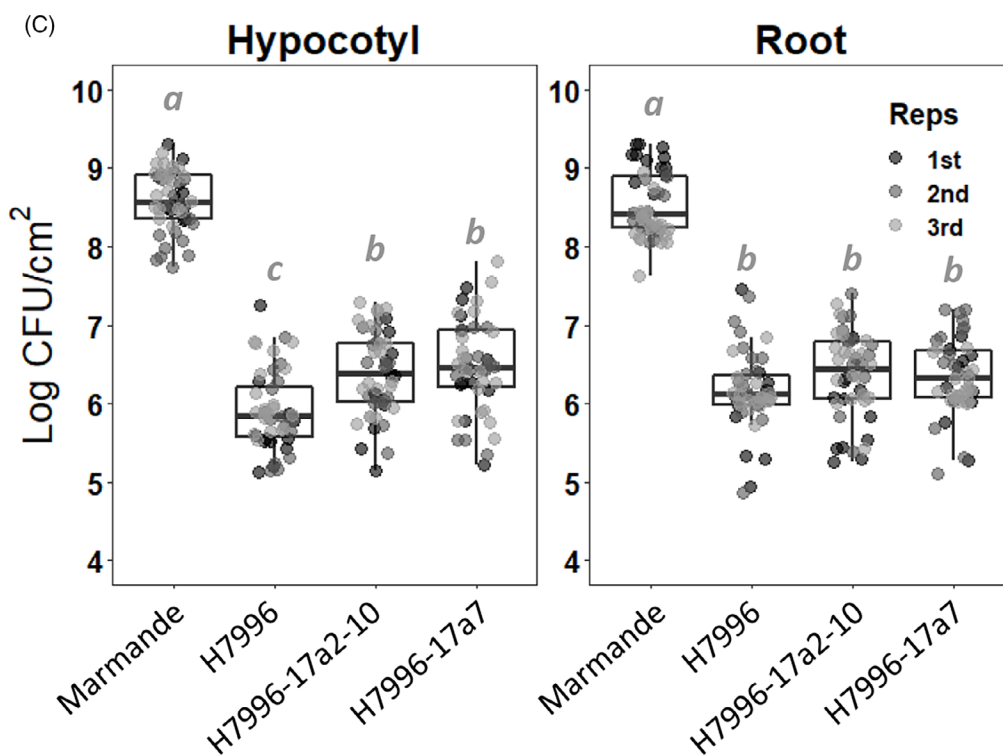
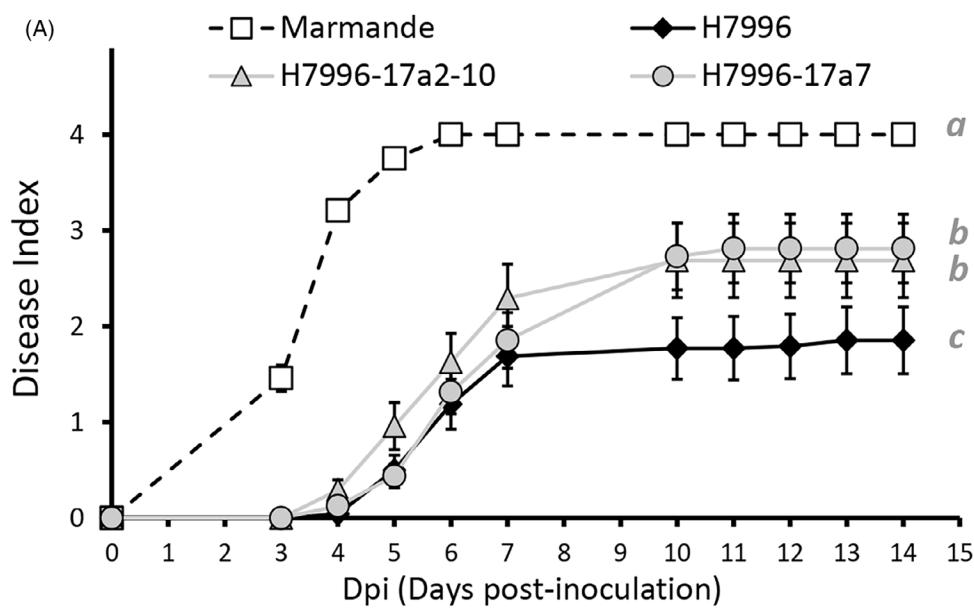


Figure 7. Pathogenicity assays of the P69D single mutant. The susceptible tomato cv Marmande, the resistant cv. Hawaii 7996 (H7996) and two independent H7996 lines with the same CRISPR mutation disrupting the P69D gene (17A2-10 and 17a7) were used.

(A) Evolution of disease symptoms over time. Three-week-old tomato plants were soil-drenched with a 10^8 CFU ml⁻¹ *Ralstonia solanacearum* suspension and wilting symptoms scored for 2 weeks. The graph shows the results of a representative experiment out of the three biological replicas performed using at least 20 plants of each variety and line.

(B) Plant phenotypes at the end of the experiment (day 14). To facilitate visualisation, plants were ranged by symptom severity within treatments before photography.

(C) Bacterial multiplication in the roots and hypocotyls of 3-week-old plants assessed 5 days after soil-drench inoculation with a luminescent *R. solanacearum* strain ($n = 16$ – 20 plants). The roots and the base of the hypocotyls were excised and bacteria was quantified by emitted luminescence and transformed to CFU ml⁻¹. Each dot shows the bacterial count in one plant. Different letters next to each graph or above each boxplot indicate statistically significant differences ($\alpha = 0.05$, Fisher's least significant difference test). The results from three independent experiments are shown as dots of different shading colours.

protease candidates with a potential role in defence against *R. solanacearum* in tomato (Planas-Marques et al., 2018). Specifically, the activity of seven P69s increased in response to the pathogen in the resistant variety Hawaii 7996 while five members of this family were also activated in susceptible plants (Figure 1d). P69D, G and J showed the highest increase in activity, and P69D was uniquely activated in the resistant cultivar (Figure 1d). We thus confined our study to the members specifically activated in the apoplast upon *R. solanacearum* infection: P69A, P69B, P69C, P69D, P69G and P69J (Figure 4). We carried out PICS to determine the substrate cleavage site of these P69s. This methodology serves as an indicator of preferred amino acids in protease cleavage sites, but it has two major limitations: (i) the short length of the peptides in the library, which facilitates access to the protease active site and (ii) the lack of other interacting proteins present *in vivo*. Our PICS results for P69A were slightly different from those previously obtained (Reichardt et al., 2018), in which a very strong preference for aspartate (close to 90%) was found in position P1. We believe that the differences between the two experiments can be attributed to the larger size of the peptide library used here, which increases the number of cleavable sequences and may favour less preferred residues. In effect, the robustness of our results is clearly exemplified by the fact that for P69D a very similar cleavage site logo is observed using PICS and the HUNTER approach, where cleavage of intact proteins was observed *in vitro* (Figure 3; Figure S6c).

P69D is the most conserved P69 gene across the four Solanaceae species investigated, and it exhibited the most distinct PICS profile (Figure 3), suggesting a function divergent from the other family members. P69B was reported to cleave aspartate residues present in the junction between the autoinhibitory prodomain of Rcr3 and its mature form, but it could also cleave synthetic peptides with an alanine residue in this position (Paulus et al., 2020). The latter observation correlates with our PICS analysis (Figure 3) and suggests that aspartic-containing proteins might not be the exclusive target(s) of P69B. Overall, P69s showed similar cleavage site selectivity and considerable cleavage promiscuity, suggesting that specificity *in vivo* may rather be provided by other mechanisms.

The tomato genome codes for 10 P69s that share more than 71% sequence identity (Reichardt et al., 2018). The highest sequence variability is observed in the protease-associated (PA) and Fn3-like domains (Figure 1C). The PA domain has been described as a protein–protein interaction module in many different and unrelated proteins, contributing to substrate recognition and selectivity (Schaller et al., 2018). In plants, the interaction between the PA domains and β -hairpin motifs of two tomato SBT3 promoters was proposed to mediate homodimerization and to regulate SBT3 activity by lifting a presumed autoinhibition (Ottmann et al., 2009). In the soybean protease C1, the PA domain was proposed to determine the length of the targeted substrates (Tan-Wilson et al., 2012) and in Arabidopsis SBT1.8, two residues of the PA domain (R302 and S333, numbers referring to the mature protease) are required for recognition of sulfo-tyrosine at the cleavage site and proteolytic maturation of the TWS1 peptide (Royek et al., 2022). In sum, the little divergence observed within the subtilase domain suggests that the PA domain might contribute to functional specialisation in different P69 family members, although differential tissue expression may also contribute to the presumed functional diversity of P69 proteins.

P69D function and mutant phenotype

P69D was found to accumulate and be activated in *R. solanacearum*-infected apoplast of resistant H7996 (Figure 1), while it was neither detected in the susceptible variety Marmande, nor in the xylem sap of any of the two varieties (our unpublished results). In order to identify P69D substrate candidates we undertook a two-pronged degradomics approach (Demir et al., 2018), comparing (i) apoplast proteome and N-terminome of P69D knockout and wild type plants *in vivo* and (ii) searching for direct P69D cleavages *in vitro*. The comparison of the apoplast proteomes indicated a lower abundance of immune-responsive proteins in P69D-deficient plants, while the N-terminome analysis showed altered proteolytic processing patterns, particularly in PR1B and PR2. Interestingly, the CAPE peptide released from the C-terminus of PR1B after wounding is a well-known immune signalling peptide (Chen et al., 2014). The altered processing of PR1B observed here therefore may perturb the release of PR1B-derived peptides -

such as CAPE- and possibly PR2-derived peptides as well. These peptides would signal plant defence responses and could contribute to the weaker immune response in P69D knockout plants. All cleavages that we observed using HUNTER were at the N-terminus of PR1B and CAPE is located at the C-terminal end. However, CAPE or any other short C-terminal peptide would most likely be undetectable because they are lost during the protein purification step after the initial HUNTER labelling. In any case, the CAPE cleavage site (CNYD-PVGN) with P at position P1' does not match the P69 PICS cleavage site profiles.

Strikingly, few P69D-dependent cleavage products accumulated after incubation with recombinant P69D in the apoplast (Figure S6a), while few N-terminal peptides derived from PR1B or PR2 cleavage were further degraded. This may indicate that (i) P69D degrades fragments of PR proteins cleaved by other proteases to attenuate generated signals, or (ii) that P69D is required to activate other proteases required for the processing of intact apoplast proteins. The related subtilase P69B has previously been shown to activate the papain-like cysteine protease Rcr3, suggesting that this may be a more general function of P69 proteases. Incubation with total leaf extracts demonstrated that recombinant P69D can cleave isolated protein *in vitro*, suggesting that the assay works (Figure S6b). However, we cannot exclude that, endogenous or bacterium-derived inhibitors were present in higher concentration in the apoplast that may have inhibited the added recombinant P69D, or that P69D may have been degraded, as we did not observe peptides mapping uniquely to P69D in these samples. Also, apoplast proteins may be stably folded in the used isolation buffer that and therefore not processed, whereas proteins in total leaf extracts may have partially denatured during isolation due to changes in pH and concentration and therefore may have been more amenable to P69D cleavage. Taken together, the proteome and N-terminome data point to widespread changes in protease activity in the apoplast of P69D-deficient plants that result in altered processing of PR1B, which likely affects immune signalling mediated by the release of CAPE or other still unknown peptides.

Phenotypic characterisation of P69-deficient plants indicates that this protein participates in the response of resistant tomato plants against *R. solanacearum* infection (Figure 7). During the early stages of colonisation, *R. solanacearum* occupies the root apoplastic space, while it is restricted to the xylem in the stem of H7996 (Planas-Marques et al., 2020). The stronger phenotype of the P69 mutation at late disease stages (wilting symptoms) and in bacterial numbers in the hypocotyl, compared to the weak effect observed in the root (Figure 7C) thus seems contradictory. However, this can be explained by an accumulative effect produced by the restriction of bacterial multiplication in the root apoplast and the other bottlenecks encountered

by the bacterium during colonisation (Planas-Marques et al., 2020). P69D-deficient plants were as susceptible as wild-type H7996 when the pathogen was directly inoculated into the stem, (Figure S7). This strengthens the role of P69D in the root apoplast during the first stages of *R. solanacearum* infection, which are overcome when the bacterium is directly injected into the stem. Interestingly, the lack of P69D did not affect the multiplication of the foliar pathogen *P. syringae* in the leaf apoplast, which hints at a specific role of this protease in the root. However, the proposed role of P69D in defence in the root does not seem to constitute a general mechanism against vascular pathogens, since P69D-deficient plants responded as WT to infection with *F. oxysporum* (Figure S8).

When it was first discovered, P69D was thought to have a role in development because of its expression in flowers, expanding cotyledons and leaves, and its lack of induction by salicylic acid or pathogen treatments (Jorda et al., 1999). This pattern of expression correlated with transcriptomic data, where *P69D* expression was particularly induced in young tissues of *S. pimpinellifolium* but not by *P. syringae* pv tomato DC3000 (<http://ted.bti.cornell.edu/>). It is tempting to speculate that a potential role of P69D in cell elongation by changing cell wall properties may have been co-opted for plant defence. P69D could indeed act as a surveillance protein that regulates downstream processes, such as cell wall remodelling to respond to pathogen attack. This correlates with the quantitative nature of bacterial wilt resistance in tomato, whereby P69D would be one of the multiple layers of defence whose absence only partially abolishes resistance (Figure 7).

MATERIALS AND METHODS

In silico analyses

BLASTn/p searches to identify tomato P69 genes were performed on the SolGenomics and NCBI databases (<https://solgenomics.net>, <https://www.ncbi.nlm.nih.gov/>). Orthologue candidates were selected as proteins with >55% identity (60% for potato) and >50% alignment score to P69C. Databases used to identify P69 orthologues in each species are indicated in Table S2, and the equivalence between gene and protein identifiers of tomato P69s in the SGN, NCBI and UniprotKB is indicated in Table S1.

P69 subtilases were located on the tomato genome using the genome browser webtools from the SGN database (Jbrowse). Neighbour-joining trees and amino acid sequence identity matrices were constructed from the respective ClustalO sequence alignments and visualised either with GSTree (<http://genestudio.com>) or iTOL (<https://itol.embl.de>).

Putative N-glycosylation sites in P69 proteins were predicted using the NetNGlyc 1.0 Server (<http://www.cbs.dtu.dk/services/NetNGlyc/>) with a threshold of significance of 0.5. Structure homology models of P69 subtilases were built in the Alpha Fold server AlphaFold2.ipynb (Mirdita et al., 2022) (<https://colab.research.google.com/github/sokrypton/ColabFold/blob/main/AlphaFold2.ipynb>). The structures were visualised with PyMOL 2.5 (<https://pymol.org/2/>).

DNA cloning and transient expression

The coding sequences (ORFs) of P69B, P69C, P69D, P69G and P69J were amplified from tomato H7996 by PCR using the primer combinations specified in Table S3 and cloned into pJET1.2/blunt (Thermo Scientific™). ORFs confirmed by Sanger sequencing were cloned downstream of the CaMV 35S promoter in pART7 (Gleave, 1992) using the restriction enzymes *Sma*I and *Bam*HI. Expression cassettes were mobilised to the binary vector pART27 (Gleave, 1992) using *Not*I. The expression vector for P69A with a C-terminal His-tag (Solyc08g079840) was previously described (Reichardt et al., 2018).

Transient expression in *N. benthamiana* was performed as previously described (Reichardt et al., 2018), with some modifications. Briefly, *Agrobacterium tumefaciens* C58C1 containing the constructs and collected from plates were resuspended in 10 ml of 10 mM MES pH 5.6, 10 mM MgCl₂. Strains were mixed to a final OD₆₀₀ of 0.7 for pART27-P69 and 0.3 for p19 and infiltrated in the leaves of 3- to 4-week-old *N. benthamiana* using a blunt syringe. Five days after agroinfiltration, leaves were harvested and the apoplastic fluid was collected in 50 mM NaH₂PO₄/Na₂HPO₄, pH 6.5, 200 mM KCl as described (Reichardt et al., 2018).

Protein purification and activity assays

Apoplastic fluids were subjected to metal chelate affinity chromatography with Ni-NTA agarose (Qiagen; Venlo, The Netherlands) on Poly-Prep® chromatography columns (Bio-Rad, Hercules, CA, USA). The apoplastic fluid obtained from P69J-expressing leaves was subjected to gel filtration using a Superdex 200 column on an Äkta Purifier chromatography system (GE Healthcare, Chicago, IL, USA). Finally, eluate fractions resulting from the affinity purification (P69A-D and P69G) and the fractions from the gel filtration purification (P69J) were concentrated using Vivaspin® concentrators (MW cutoff 10 kDa; Sartorius Stedim Biotech, Aubagne, France).

Activity of recombinant P69s was monitored using a fluorogenic 11-mer peptide (aminobenzoyl-SKRDPKMQTD(NO₂)Y) (JPT Peptide Technologies, Berlin, Germany) and casein as substrates at 25 μM and 10 μg ml⁻¹, respectively. Assays were performed in 50 mM acetic acid, 50 mM MES, 100 mM Tris/HCl (pH 7.5 unless otherwise indicated) and relative fluorescence increase was monitored using a SPARK® microplate reader (Tecan; Männedorf, Switzerland).

For substrate identification *in vitro*, recombinant P69D purified from *N. benthamiana* was incubated with total or apoplast protein extracts for 30 min at RT at an enzyme: proteome ratio of 1:200. No apparent overall protein degradation was observed in these conditions.

PICS analyses

Proteomics Identification of Cleavage Sites (Schilling et al., 2011; Schilling & Overall, 2008) was used to analyse the substrate specificity of tomato P69s, with slight modifications detailed in (Reichardt et al., 2018). Hundred micrograms of the chemically modified peptide library was digested at 25°C with purified P69s in 50 mM NaH₂PO₄/Na₂HPO₄, pH 6.5, at an enzyme to library ratio of 1:1000 (w/w) for 2 h. Purified peptides were subjected to LC-MS/MS and cleavage sites were reconstructed using WebPICS. (<http://clipserve.dentistry.ubc.ca/pics>) and cleavage specificity preferences were visualised using IceLogos (<https://iomics.ugent.be/icelogoserver/>) (Colaert et al., 2009).

Proteome and N-terminome sample preparation

For quantitative analysis of the apoplast proteomes, purified proteins were dissolved and denatured in 6 M guanidine buffered with

100 mM HEPES to pH 7.2, cysteine residues reduced with 10 mM DTT and alkylated with 30 mM IAA and digested with proteomics-grade trypsin at an enzyme:proteome ratio of 1:100 for 16 h at 37°C. Peptides were differentially stable isotopes labelled by reductive dimethylation (Boersema et al., 2009) with light labelling (20 mM CH₂O and 20 mM NaBH₃CN, +28.0313 Da) of wild type proteomes and heavy isotope labelling (20 mM ¹³CD₂O and 20 mM NaBH₃CN, +34.0631 Da) of 17a7 P69D knockout proteomes. Labelling reactions were incubated for 3 h at 37°C, then quenched with 100 mM Tris-HCl pH 6.8 for 1 h at RT, pooled, purified using reverse-phase STAGE tips (Rappsilber et al., 2007), dried in a vacuum concentrator and reconstituted in 0.1% formic acid prior to LC/MS analysis.

HUNTER N-terminome analyses were performed as described (Demir et al., 2022). Briefly, free primary amines at the protein N-termini and lysine side chains were differentially stable isotope-labelled by reductive dimethylation, using the light isotopes for WT and heavy isotope for 17A7 proteomes for the *in vivo* experiment. In the *in vitro* experiments, proteomes treated with a mock-purified *N. benthamiana* apoplast extract were labelled with light isotopes and proteomes treated with enriched recombinant P69D were labelled with heavy isotopes. Proteins were then digested with trypsin and new peptide alpha-amines generated by the tryptic digest were modified with undecanal. N-terminal peptides were then selectively enriched by depletion of the undecanal-modified peptides using HRX reverse-phase cartridges (Macherey and Nagel, Düren, Germany). Enriched N-terminal peptides were desalted with STAGE tips as described above.

Mass spectrometry data analysis

Peptides were analysed using an UltiMate 3000 RSCL nano-HPLC system (Thermo Fisher Scientific, Waltham, MA, USA) online coupled to an Impact II Q-TOF mass spectrometer (Bruker Scientific Instruments; Billerica, MA, USA) via a CaptiveSpray ion source boosted with an ACN-saturated nitrogen gas stream as described (Beck et al., 2015). Peptides were loaded on a μPAC pillar array trap column (1 cm length; PharmaFluidics; Zwijnaarde, Belgium) and separated on a μPAC pillar array analytical column (50 cm flowpath; PharmaFluidics) using a 2 h elution protocol that included an 80 min separation gradient from 5% to 35% solvent B (solvent A: H₂O + 0.1% FA, solvent B: ACN + 0.1% FA) at a flow rate of 300 nl min⁻¹ at 60°C. Line-mode MS spectra were acquired in mass range of 200–1400 m/z with a Top14 method.

Acquired tandem mass spectra were queried with MaxQuant (Tyanova et al., 2016) v.2.0.3 against a database consisting of the UniProt *R. solanacearum* database (release 2022_04) and the UniProt *S. lycopersicum* database (release 2023_03), with the seven entries A0A3Q7HVI0, A0A3Q7HTM2, A0A3Q7HVI4, A0A3Q7F3D9, A0A3Q7HHX1, A0A3Q7HI18 and A0A3Q7HKM1 (incorrect annotations of P69 sequences) replaced by the eight P69 sequences listed in Figure 1 downloaded from the Solanaceae Genomics Network (see above) and entry A0A3Q7HXW1 (incorrect annotation of PR1 proteins as fusion protein) removed and replaced by manually annotated PR1 protein homologue sequences (12 entries). For the apoplast shotgun proteome analysis, duplex dimethyl labelling at Lys and peptide N-termini was set as label, trypsin as digestion protease with up to three missed cleavage sites, and label-free quantification enabled. Protein quantification required one unique peptide per protein group, razor proteins were not used for abundance calculations. Shotgun data analysis was based on the individual LFQ intensities of heavy and light channels to allow for imputation of missing values and determination of differentially expressed proteins using the LIMMA-moderated *t*

test as plug.in in Perseus (Yu et al., 2020) v. 2.0.10.0. For HUNTER data, search settings were set as described (Demir et al., 2022) and MaxQuant results further analysed using MANTI (Demir et al., 2021) using the graphical user interface as implemented in v5.4 (Demir & Huesgen, 2022). For *in vivo* comparisons, the π value, calculated by multiplying the fold change as a measure of protein abundance with the $-\log$ limma-moderated *t*-test *P*-value, was used as a test criterion (Xiao et al., 2014). Proteins were considered significantly different in abundance at $\pi > 1.1082$ or < -1.1082 . For *in vitro* experiments, N-terminal peptide abundance was considered significantly different at a >2 -fold change and a limma-moderated *P*-value < 0.05 .

Plant material and growth conditions

The tomato (*S. lycopersicum*) susceptible variety Marmande and the highly resistant line Hawaii 7996 were used. To generate the CRISPR/Cas9 mutant in the Hawaii7996 background (designated 17a7 and 17a2-10), single guide RNA (sgRNA) sequences were designed with high specificity score and the lowest number of off-targets using CRISPOR (Haeussler et al., 2016), synthesised (Integrated DNA Technologies; Coralville, IA, USA) and cloned as described (Danilo et al., 2018) (Table S3). The Hawaii 7996 genotype was transformed using *A. tumefaciens* C58 pGV2260 (Mazier et al., 2011). Leaf samples from regenerating plants or their progenies were screened by PCR using specific primers (Table S3). Deletions were confirmed by DNA sequencing (Macrogen, Seoul, Republic of Korea).

Plants were grown in controlled growth chambers at 60% relative humidity, 12 h:12 h, day:night and 27°C (light-emitting diode lighting) or 25°C (fluorescent lighting). Three-week-old plants were used for pathogenicity assays and developmental observation.

Bacterial material and pathogenicity assays

An *R. solanacearum* luminescent reporter derivative carrying the *PpsbA::LuxCDABE* construct (Cruz et al., 2014) was used for all experiments carried out with the wild type GMI1000 strain. Multiplication of *R. solanacearum* in *N. benthamiana* leaves was analysed using a $\Delta avrA$ and $\Delta popP1$ mutant, pathogenic on this plant and bacterial multiplications were tested at 3 dpi as previously determined (Poueymiro et al., 2009). *R. solanacearum* was routinely grown on rich B medium (10 g L⁻¹ bactopeptone, 1 g L⁻¹ yeast extract and 1 g L⁻¹ casaminoacids) using gentamicin (10 µg ml⁻¹) for selection.

For soil-drenching inoculations, plants were inoculated by pouring 40 ml of a 10⁸ CFU ml⁻¹ bacterial suspension on every pot after root wounding (Planas-Marques et al., 2020). For petiole inoculation, 10 µl of a 10⁶ CFU ml⁻¹ suspension was placed onto the petiole-stem boundary in the cotyledons or first internode and poked into the stem with a needle. Infected plants were scored for wilting symptoms using a scale from 0 to 4, where 0 = healthy plant with no wilt, 1 = 25%, 2 = 50%, 3 = 75% and 4 = 100% of the canopy wilted. For bacterial inoculation in the apoplast, plants were vacuum-infiltrated with a bacterial suspension of 10⁵ CFU ml⁻¹ as described (Planas-Marques et al., 2018). Assessment of bacterial multiplication was performed in four independent plants per time point per genotype as follows: four 5 mm-diameter leaf disks were excised from each plant. CFUs in homogenised leaf samples were counted and bacterial growth was calculated as CFU cm⁻² of leaf.

Fusarium inoculation assay

Fungal strains *FoI007* and *FoI029* were inoculated from glycerol stocks to potato dextrose agar (Becton, Dickinson and Company;

Franklin Lakes, NJ, USA) and grown for 5 days at 25°C in darkness (Marlatt et al., 1996; Mes et al., 1999). A single agar plug (~1 cm²) was put into a 250 ml flask containing 100 ml of minimal nitrate liquid medium (100 mM KNO₃, 3% sucrose and 0.17% Yeast Nitrogen Base without amino acids or ammonia) and placed in a shaker incubator (25°C). Five days after inoculation, the fungal suspension was filtered through sterile miracloth (Merck Millipore; Burlington, MA, USA), spinned down, washed and diluted with sterilised Milli-Q water (10⁷ spores ml⁻¹) (Rep et al., 2004). Ten-day-old tomato cv. Hawaii 7996 (H7996) and CRISPR/Cas9 knock-out lines were uprooted and trimmed (remaining root length approx. 1.5 cm long). Seedlings were root dip inoculated by placing them for 2 min in water (mock) or the spore suspension. The plants were grown in a greenhouse at 25°C, 65% relative humidity and a 16-h photoperiod. Three weeks post-inoculation fresh weight and disease index were scored as described (de Lamo et al., 2021). Statistical analyses were done using the software PRISM 9.3.0 (GraphPad).

P. syringae inoculation assay

Three-week-old tomato plants Hawaii 7996 (H7996) and CRISPR/Cas9 knockout lines were grown at 25°C with constant light conditions (12 h light, 12 h darkness). *P. syringae* pv. tomato DC3000 strain was grown on selective King's B medium (Merck Millipore; Burlington, MA, USA) plates for 48 h at 28°C. Bacteria was then resuspended in 10 mM MgCl₂ with 0.002% Silwet I-77 to 10⁵ CFU ml⁻¹ (OD₆₀₀ = 0.0002), and the aerial part of the plants was vacuum-infiltrated with the bacterial suspension for ~20 sec. Bacterial loads were measured by sampling four 5-mm leaf discs per biological replicate at 0 and 3 dpi. Samples were homogenised and 10 µl of serial 10-fold dilutions were plated in selective plates to count CFUs and bacterial growth was calculated as CFU cm⁻² of leaf.

Statistical analyses

Statistical analyses were performed using the STATGRAPHICS Centurion XVI software. All statistical tests are indicated in the respective figure legends.

AUTHOR CONTRIBUTIONS

Conceptualization: MV and NSC; methodology: MV, NSC, ASt, FLWT, MaM, PFH; investigation: WZ, MP-M, ASt, MS, MaM, MeM; writing—original draft preparation: MV; writing—review and editing: NSC, WZ, ASt, ASc, MS, FLWT, PFH; funding acquisition: NSC, MV, ASc, FLWT, PFH.

ACKNOWLEDGEMENTS

The authors would like to thank all members of the Bacterial plant diseases and cell death lab for helpful comments and Fabien Nogue for smart advice about sgRNA design. Research was funded by grant MCIN/AEI/PID2019-108595RB-I00 funded by MCIN/AEI/10.13039/501100011033 (to N.S.C. and M.V.), grant TED2021-131457B-I00 funded by MCIN/AEI/10.13039/501100011033 and by the 'European Union NextGenerationEU/PRTR' (to N.S.C. and M.V.), through the 'Severo Ochoa Programme for Centres of Excellence in R&D' (CEX2019-000917 funded by MCIN/AEI/10.13039/501100011033), and by the CERCA Program of the Catalan government (Generalitat de Catalunya). M.S. and F.L.W.T. obtained support from the NWO-Earth and Life Sciences funded VICI Project No. 865.14.003. W.Z. was the recipient of a CSC Fellowship CSC201906990041. M.P.-M. was the recipient of an FPU grant (FPU15/02125) funded by Ministerio de Universidades. GAFL

UR1052 benefits from the support of the French National Agency (ANR11-BTBR-0001-GENIUS). We acknowledge the support of the publication fee by the CSIC Open Access Publication Support Initiative through its Unit of Information Resources for Research (URIC).

CONFLICT OF INTEREST

The authors declare no conflicts of interest.

DATA AVAILABILITY STATEMENT

The mass spectrometry proteomics data have been deposited to the ProteomeXchange Consortium (Deutsch et al., 2023) via the PRIDE partner repository (Perez-Riverol et al., 2022) with the dataset identifiers PXD044635 for the comparison of WT and the *p69d* mutant proteomes and PXD044637 for the *in vitro* N-terminomes generated after incubation of apoplast proteome with recombinant P69D. Other data that support the findings of this study are available from the corresponding authors upon reasonable request.

SUPPORTING INFORMATION

Additional Supporting Information may be found in the online version of this article.

Figure S1. Phylogenetic analysis of the conserved P69 clade across different Solanaceae species. Neighbour-joining protein similarity trees generated from a ClustalO alignment of protein sequences sharing >55% identity with P69C (>60% identity for potato) and >50% of the alignment's maximum score. Identified P69 clades in each species are coloured, while non-P69 subtilases are shown in grey. Scale bar indicates 0.1 nucleotide changes.

Figure S2. Identification of the putative tomato P69 homologues in sequenced Solanaceae genomes. Neighbour-joining phylogenetic tree (a) and amino acid sequence identity matrix (b) generated from a ClustalO alignment of the proposed P69 protein sequences from tomato (P69), potato ('DMP'), eggplant ('SMEL'), pepper ('CA'), *N. tabacum* ('Nitab') and *N. attenuata* ('NIAT'). P69 orthologues are coloured in red (tomato), brown (potato), purple (eggplant) and orange (pepper) in the tree. Scale bar indicates 0.1 changes per site per 100 nucleotides. Numbers in the table indicate percentage identity to the orthologue in tomato. n/p, not present according to our percentage identity criteria.

Figure S3. Purification of recombinant P69 enzymes. (a) Tomato P69A to D, P69G and P69J were transiently expressed in *N. benthamiana* leaves by agroinfiltration, the apoplastic fluids were collected 5 days later and subjected to metal chelate affinity chromatography. Fractions of each purification step were analysed by SDS-PAGE. An empty vector (EV) was included as a control. (b) Gel filtration chromatography of apoplastic fluid collected from P69J-expressing leaves. Eluate fractions 1–4 (a) and gel filtration fractions 25–33 (b) were pooled and concentrated using centrifugal concentrators.

Figure S4. Analysis of putative P69G *N*-glycosylation sites. (a) Putative *N*-glycosylation sites predicted on mature P69G with NetNGlyc 1.0 Server (<http://www.cbs.dtu.dk/services/NetNGlyc/>) using a threshold of 0.5 significance. P69B was included as a control. Amino acid sequences were aligned by ClustalW and visualised using MEGA-X (<https://www.megasoftware.net/>). Asparagine residues (N) predicted to be *N*-glycosylated are indicated by numbered position on the aligned sequences. Experimentally proven

glycosylation sites in P69B are marked in bold. (b) Comparison of predicted glycosylations and detected P69G protein species. Left panel: Glycan composition and estimated molecular mass of differentially glycosylated asparagine residues detected by Bykova et al. (2006) in P69B. In bold, most abundant glycan structure based on relative intensities of ion peaks. Centre panel: predicted molecular weights of P69D variants fused with His-tag modified at all putative *N*-glycosylation sites with the lightest, the most abundant and the heaviest glycan. Right image, SyproRuby-stained SDS-PAGE of purified hexa-His-tagged P69D. Arrowheads indicate apparent mass for the observed protein bands.

Figure S5. Generation of a *p69d* CRISPR/Cas9 deletion mutant. (a) Schematic representation showing the 202 bp deletion obtained by CRISPR/Cas9 in the P69D gene. The mutation results in a premature stop codon, resulting in a truncated protein variant. D, H and S indicate the putative aspartate, histidine and serine residues from the active site. Arrowheads indicate genotyping primers (F, Forward; R, Reverse). Dashed lines indicate the double-strand break site used by Cas9. (b) Phenotype of Hawaii 7996 tomato plants and the derived P69D mutant lines. Representative pictures and fresh weight of the wild type Hawaii 7996 (H7996) and the two genome-edited plant lines used in this work 3 weeks after germination.

Figure S6. N-terminome analysis of P69D-deficient plants after incubation with recombinant P69D *in vitro*. (a) Volcano plot depicting N-terminal peptide abundance in apoplastic extracts from P69D-deficient plants infected with *R. solanacearum* after incubation with recombinant P69D (P69D) or empty vector control (EV). Open circles, N-termini mapping to canonical protein termini mapping to positions 1 or 2 with intact or removed Met, known signal- or transit peptide sequences; filled circles, non-canonical protein termini mapping to positions within their protein sequence; red and blue, N-terminal peptides significantly accumulating or depleted (moderated t-test *P*-value < 0.05, twofold change in abundance) after incubation with recombinant P69D. (b) Volcano plot depicting changes in N-terminal peptide abundance after incubation of total leaf proteome isolated from *R. solanacearum*-infected P69D-deficient plants with recombinant P69D or mock purification after empty vector (EV) expression as control. Open circles, N-termini mapping to canonical protein termini mapping to positions 1 or 2 with intact or removed Met, known signal- or transit peptide sequences; filled circles, non-canonical protein termini mapping to positions within their protein sequence; red and blue, N-terminal peptides significantly accumulating or depleted (moderated t-test *p*-value < 0.05, twofold change in abundance) after incubation with recombinant P69D. (c) Icelogo depicting the amino acid prevalence of 133 aligned P69D cleavage sites derived from dimethylated, non-canonical N-terminal peptides identified in (b).

Figure S7. Pathogenicity assays of the P69D single mutant by petiole-inoculation. Four or 6-week-old tomato plants were petiole-inoculated with 10^6 CFU ml⁻¹ *R. solanacearum* suspension as indicated. Wilting symptoms were scored over time for 2 weeks. The graph shows the results of a representative experiment out of the three biological replicas performed using at least 20 plants of each variety and line. Different letters next to each graph or above each boxplot indicate statistically significant differences ($\alpha = 0.05$, Fisher's least significant difference test).

Figure S8. *Fusarium* and *Pseudomonas* disease assay of CRISPR/Cas9 *p69d* KO lines. Ten-day-old Hawaii 7996 (H7996) and the P69D knockout tomato lines were root dip inoculated with mock, *Fol1007* or *Fol029*. Three weeks post-inoculation five representative plants per treatment were photographed (a), their fresh weight was measured (b) and disease index (c) were scored on a scale from 0 (healthy plant) to 5 (dead plant). Statistical analyses were

performed using an Ordinary One-way ANOVA for fresh weight and a Mann–Whitney U test for disease index data. The assay was repeated twice using approximately 20 plants per treatment yielding similar results. Three-week-old Hawaii 7996 (H7996) and the P69D knockout tomato lines were inoculated with *P. syringae* pv. tomato DC3000 by leaf infiltration and bacterial loads were measured at 0 and 3 dpi. Eight biological replicates were used.

Table S1. Gene and protein identifiers for tomato P69s.

Table S2. Databases used for the construction of P69-like gene phylogeny in Solanaceae species.

Table S3. Oligonucleotides used in this study.

Data S1. List of apoplastic proteins *in vivo*.

Data S2. List of apoplastic N-termini *in vivo*.

Data S3. List of apoplastic N-termini *in vitro*.

Data S4. List of apoplastic N-termini *in vitro*.

REFERENCES

- Beck, S., Michalski, A., Raether, O., Lubeck, M., Kaspar, S., Goedecke, N. *et al.* (2015) The impact II, a very high-resolution quadrupole time-of-flight instrument (QTOF) for deep shotgun proteomics. *Molecular & Cellular Proteomics*, **14**(7), 2014–2029.
- Boersema, P.J., Raijmakers, R., Lemeer, S., Mohammed, S. & Heck, A.J. (2009) Multiplex peptide stable isotope dimethyl labeling for quantitative proteomics. *Nature Protocols*, **4**(4), 484–494.
- Bykova, N.V., Rampitsch, C., Krokhin, O., Standing, K.G. & Ens, W. (2006) Determination and characterization of site-specific N-glycosylation using MALDI-Qq-TOF tandem mass spectrometry: case study with a plant protease. *Analytical Chemistry*, **78**(4), 1093–1103.
- Cedzich, A., Huttenlocher, F., Kuhn, B.M., Pfannstiel, J., Gabler, L., Stintzi, A. *et al.* (2009) The protease-associated domain and C-terminal extension are required for zymogen processing, sorting within the secretory pathway, and activity of tomato subtilase 3 (SISBT3). *The Journal of Biological Chemistry*, **284**(21), 14068–14078.
- Chen, Y.L., Lee, C.Y., Cheng, K.T., Chang, W.H., Huang, R.N., Nam, H.G. *et al.* (2014) Quantitative peptidomics study reveals that a wound-induced peptide from PR-1 regulates immune signaling in tomato. *The Plant Cell*, **26**(10), 4135–4148.
- Chichkova, N.V., Shaw, J., Galiullina, R.A., Drury, G.E., Tuzhikov, A.I., Kim, S.H. *et al.* (2010) Phytaspase, a localisable cell death promoting plant protease with caspase specificity. *The EMBO Journal*, **29**(6), 1149–1161.
- Colaert, N., Helsens, K., Martens, L., Vandekerckhove, J. & Gevaert, K. (2009) Improved visualization of protein consensus sequences by ice-Logo. *Nature Methods*, **6**(11), 786–787.
- Cruz, A.P., Ferreira, V., Pianzola, M.J., Siri, M.I., Coll, N.S. & Valls, M. (2014) A novel, sensitive method to evaluate potato germplasm for bacterial wilt resistance using a luminescent *Ralstonia solanacearum* reporter strain. *Molecular Plant-Microbe Interactions*, **27**(3), 277–285.
- Danilo, B., Perrot, L., Botton, E., Nogue, F. & Mazier, M. (2018) The DFR locus: a smart landing pad for targeted transgene insertion in tomato. *PLoS One*, **13**(12), e0208395.
- de Lamo, F.J., Constantin, M.E., Fresno, D.H., Boeren, S., Rep, M. & Takken, F.L.W. (2018) Xylem sap proteomics reveals distinct differences between R gene- and endophyte-mediated resistance against *Fusarium* wilt disease in tomato. *Frontiers in Microbiology*, **9**, 2977.
- de Lamo, F.J., Simkovicova, M., Fresno, D.H., de Groot, T., Tintor, N., Rep, M. *et al.* (2021) Pattern-triggered immunity restricts host colonization by endophytic fusaria, but does not affect endophyte-mediated resistance. *Molecular Plant Pathology*, **22**(2), 204–215.
- Demir, F. & Huesgen, P.F. (2022) A user guide to validation, annotation, and evaluation of N-Terminome datasets with MANTI. *Methods in Molecular Biology*, **2447**, 271–283.
- Demir, F., Kizhakkedathu, J.N., Rinschen, M.M. & Huesgen, P.F. (2021) MANTI: automated annotation of protein N-termini for rapid interpretation of N-Terminome data sets. *Analytical Chemistry*, **93**(13), 5596–5605.
- Demir, F., Niedermaier, S., Villamor, J.G. & Huesgen, P.F. (2018) Quantitative proteomics in plant protease substrate identification. *The New Phytologist*, **218**(3), 936–943.
- Demir, F., Perrar, A., Mantz, M. & Huesgen, P.F. (2022) Sensitive plant N-terminome profiling with HUNTER. *Methods in Molecular Biology*, **2447**, 139–158.
- Deutsch, E.W., Bandeira, N., Perez-Riverol, Y., Sharma, V., Carver, J.J., Mendonza, L. *et al.* (2023) The ProteomeXchange consortium at 10 years: 2023 update. *Nucleic Acids Research*, **51**(D1), D1539–D1548.
- Du, Y., Stegmann, M. & Misas Villamil, J.C. (2016) The apoplast as battleground for plant-microbe interactions. *The New Phytologist*, **209**(1), 34–38.
- French, E., Kim, B.S., Rivera-Zuluaga, K. & Iyer-Pascuzzi, A.S. (2018) Whole root transcriptomic analysis suggests a role for auxin pathways in resistance to *Ralstonia solanacearum* in tomato. *Molecular Plant-Microbe Interactions*, **31**(4), 432–444.
- Gawehns, F., Ma, L., Bruning, O., Houterman, P.M., Boeren, S., Cornelissen, B.J. *et al.* (2015) The effector repertoire of *Fusarium oxysporum* determines the tomato xylem proteome composition following infection. *Frontiers in Plant Science*, **6**, 967.
- Gleave, A.P. (1992) A versatile binary vector system with a T-DNA organizational structure conducive to efficient integration of cloned DNA into the plant genome. *Plant Molecular Biology*, **20**(6), 1203–1207.
- Granell, A., Bellés, J.M. & Conejero, V. (1987) Induction of pathogenesis-related proteins in tomato by citrus exocortis viroid, silver ion and ethphon. *Physiological and Molecular Plant Pathology*, **31**(1), 83–90.
- Grimault, V., Gélie, B., Lemattre, M., Prior, P. & Schmit, J. (1994) Comparative histology of resistant and susceptible tomato cultivars infected by *Pseudomonas solanacearum*. *Physiological and Molecular Plant Pathology*, **44**, 105–123.
- Gupta, R., Lee, S.E., Agrawal, G.K., Rakwal, R., Park, S., Wang, Y. *et al.* (2015) Understanding the plant–pathogen interactions in the context of proteomics-generated apoplastic proteins inventory. *Frontiers in Plant Science*, **6**, 352.
- Haeussler, M., Schonig, K., Eckert, H., Eschstruth, A., Mianne, J., Renaud, J.B. *et al.* (2016) Evaluation of off-target and on-target scoring algorithms and integration into the guide RNA selection tool CRISPOR. *Genome Biology*, **17**(1), 148.
- Hayward, A.C. (1991) Biology and epidemiology of bacterial wilt caused by *Pseudomonas solanacearum*. *Annual Review of Phytopathology*, **29**, 65–87.
- Homma, F., Huang, J. & van der Hoorn, R.A.L. (2023) AlphaFold-multimer predicts cross-kingdom interactions at the plant–pathogen interface. *bioRxiv*. 2023.2023.04.03.535425.
- Ishihara, T., Mitsuhara, I., Takahashi, H. & Nakaho, K. (2012) Transcriptome analysis of quantitative resistance-specific response upon *Ralstonia solanacearum* infection in tomato. *PLoS One*, **7**(10), e46763.
- Jorda, L., Coego, A., Conejero, V. & Vera, P. (1999) A genomic cluster containing four differentially regulated subtilisin-like processing protease genes in tomato plants. *The Journal of Biological Chemistry*, **274**(4), 2360–2365.
- Jorda, L., Conejero, V. & Vera, P. (2000) Characterization of P69E and P69F, two differentially regulated genes encoding new members of the subtilisin-like proteinase family from tomato plants. *Plant Physiology*, **122**(1), 67–74.
- Macho, A.P. & Zipfel, C. (2014) Plant PRRs and the activation of innate immune signaling. *Molecular Cell*, **54**(2), 263–272.
- Mahon, P. & Bateman, A. (2000) The PA domain: a protease-associated domain. *Protein Science*, **9**(10), 1930–1934.
- Marlatt, M., Correll, J.C., Kaufmann, P. & Cooper, P. (1996) Two genetically distinct populations of *Fusarium oxysporum* f.sp. *lycopersicirace* 3 in the United States. *Plant Disease*, **80**(12), 1336.
- Mazier, M., Flamain, F., Nicolai, M., Sarnette, V. & Caranta, C. (2011) Knockdown of both eIF4E1 and eIF4E2 genes confers broad-spectrum resistance against potyvirus in tomato. *PLoS One*, **6**(12), e29595.
- Meichtry, J., Amrhein, N. & Schaller, A. (1999) Characterization of the subtilase gene family in tomato (*Lycopersicon esculentum* Mill.). *Plant Molecular Biology*, **39**(4), 749–760.
- Mes, J.J., Weststeijn, E.A., Herlaar, F., Lambalk, J.J., Wijbrandi, J., Haring, M.A. *et al.* (1999) Biological and molecular characterization of *Fusarium oxysporum* f.sp. *lycopersici* divides race 1 isolates into separate virulence groups. *Phytopathology*, **89**(2), 156–160.
- Meyer, M., Leptihn, S., Welz, M. & Schaller, A. (2016) Functional characterization of propeptides in plant Subtilases as intramolecular chaperones

- and inhibitors of the mature protease. *The Journal of Biological Chemistry*, **291**(37), 19449–19461.
- Mirdita, M., Schutze, K., Moriwaki, Y., Heo, L., Ovchinnikov, S. & Steinegger, M. (2022) ColabFold: making protein folding accessible to all. *Nature Methods*, **19**(6):679–+, 679–682.
- Muller, L., Cameron, A., Fortenberry, Y., Apletalina, E.V. & Lindberg, I. (2000) Processing and sorting of the prohormone convertase 2 propeptide. *The Journal of Biological Chemistry*, **275**(50), 39213–39222.
- Nebes, V.L. & Jones, E.W. (1991) Activation of the proteinase B precursor of the yeast *Saccharomyces cerevisiae* by autocatalysis and by an internal sequence. *The Journal of Biological Chemistry*, **266**(34), 22851–22857.
- Ottmann, C., Rose, R., Huttenlocher, F., Cedzich, A., Hauske, P., Kaiser, M. *et al.* (2009) Structural basis for Ca²⁺-independence and activation by homodimerization of tomato subtilase 3. *Proceedings of the National Academy of Sciences of the United States of America*, **106**(40), 17223–17228.
- Paulus, J.K., Kourelis, J., Ramasubramanian, S., Homma, F., Godson, A., Horger, A.C. *et al.* (2020) Extracellular proteolytic cascade in tomato activates immune protease Rcr3. *Proceedings of the National Academy of Sciences of the United States of America*, **117**(29), 17409–17417.
- Perez-Riverol, Y., Bai, J., Bandla, C., Garcia-Seisdedos, D., Hewapathirana, S., Kamatchinathan, S. *et al.* (2022) The PRIDE database resources in 2022: a hub for mass spectrometry-based proteomics evidences. *Nucleic Acids Research*, **50**(D1), D543–D552.
- Planas-Marques, M., Bernardo-Faura, M., Paulus, J., Kaschani, F., Kaiser, M., Valls, M. *et al.* (2018) Protease activities triggered by *Ralstonia solanacearum* infection in susceptible and tolerant tomato lines. *Molecular & Cellular Proteomics*, **17**(6), 1112–1125.
- Planas-Marques, M., Kressin, J.P., Kashyap, A., Panthee, D.R., Louws, F.J., Coll, N.S. *et al.* (2020) Four bottlenecks restrict colonization and invasion by the pathogen *Ralstonia solanacearum* in resistant tomato. *Journal of Experimental Botany*, **71**(6), 2157–2171.
- Poueymiro, M., Cunnac, S., Barberis, P., Deslandes, L., Peeters, N., Cazale-Noel, A.C. *et al.* (2009) Two type III secretion system effectors from *Ralstonia solanacearum* GMI1000 determine host-range specificity on tobacco. *Molecular Plant-Microbe Interactions*, **22**(5), 538–550.
- Power, S.D., Adams, R.M. & Wells, J.A. (1986) Secretion and autoproteolytic maturation of subtilisin. *Proceedings of the National Academy of Sciences of the United States of America*, **83**(10), 3096–3100.
- Rappsilber, J., Mann, M. & Ishihama, Y. (2007) Protocol for micro-purification, enrichment, pre-fractionation and storage of peptides for proteomics using StageTips. *Nature Protocols*, **2**(8), 1896–1906.
- Reichardt, S., Reppe, D., Tuzhikov, A.I., Galiullina, R.A., Planas-Marques, M., Chichkova, N.V. *et al.* (2018) The tomato subtilase family includes several cell death-related proteinases with substrate specificity. *Scientific Reports*, **8**(1), 10531.
- Rep, M., van der Does, H.C., Meijer, M., van Wijk, R., Houterman, P.M., Dekker, H.L. *et al.* (2004) A small, cysteine-rich protein secreted by *Fusarium oxysporum* during colonization of xylem vessels is required for I-3-mediated resistance in tomato. *Molecular Microbiology*, **53**(5), 1373–1383.
- Royek, S., Bayer, M., Pfannstiel, J., Pleiss, J., Ingram, G., Stintzi, A. *et al.* (2022) Processing of a plant peptide hormone precursor facilitated by posttranslational tyrosine sulfation. *Proceedings of the National Academy of Sciences of the United States of America*, **119**(16), e2201195119.
- Schaller, A., Stintzi, A., Rivas, S., Serrano, I., Chichkova, N.V., Vartapetian, A.B. *et al.* (2018) From structure to function – a family portrait of plant subtilases. *The New Phytologist*, **218**(3), 901–915.
- Schilling, O., Huesgen, P.F., Barre, O., Auf dem Keller, U. & Overall, C.M. (2011) Characterization of the prime and non-prime active site specificities of proteases by proteome-derived peptide libraries and tandem mass spectrometry. *Nature Protocols*, **6**(1), 111–120.
- Schilling, O. & Overall, C.M. (2008) Proteome-derived, database-searchable peptide libraries for identifying protease cleavage sites. *Nature Biotechnology*, **26**(6), 685–694.
- Smith, E.L., Markland, F.S., Kasper, C.B., DeLange, R.J., Landon, M. & Evans, W.H. (1966) The complete amino acid sequence of two types of subtilisin, BPN and Carlsberg. *The Journal of Biological Chemistry*, **241**(24), 5974–5976.
- Song, J., Win, J., Tian, M., Schornack, S., Kaschani, F., Ilyas, M. *et al.* (2009) Apoplastic effectors secreted by two unrelated eukaryotic plant pathogens target the tomato defense protease Rcr3. *Proceedings of the National Academy of Sciences of the United States of America*, **106**(5), 1654–1659.
- Tan-Wilson, A., Bandak, B. & Prabu-Jeyabalan, M. (2012) The PA domain is crucial for determining optimum substrate length for soybean protease C1: structure and kinetics correlate with molecular function. *Plant Physiology and Biochemistry*, **53**, 27–32.
- Tian, M., Benedetti, B. & Kamoun, S. (2005) A second Kazal-like protease inhibitor from *Phytophthora infestans* inhibits and interacts with the apoplastic pathogenesis-related protease P69B of tomato. *Plant Physiology*, **138**(3), 1785–1793.
- Tian, M., Huitema, E., Da Cunha, L., Torto-Alalibo, T. & Kamoun, S. (2004) A Kazal-like extracellular serine protease inhibitor from *Phytophthora infestans* targets the tomato pathogenesis-related protease P69B. *The Journal of Biological Chemistry*, **279**(25), 26370–26377.
- Tian, M., Win, J., Song, J., van der Hoorn, R., van der Knaap, E. & Kamoun, S. (2007) A *Phytophthora infestans* cystatin-like protein targets a novel tomato papain-like apoplastic protease. *Plant Physiology*, **143**(1), 364–377.
- Tornero, P., Conejero, V. & Vera, P. (1997) Identification of a new pathogen-induced member of the subtilisin-like processing protease family from plants. *The Journal of Biological Chemistry*, **272**(22), 14412–14419.
- Tornero, P., Mayda, E., Gomez, M.D., Canas, L., Conejero, V. & Vera, P. (1996) Characterization of LRP, a leucine-rich repeat (LRR) protein from tomato plants that is processed during pathogenesis. *The Plant Journal*, **10**(2), 315–330.
- Tyanova, S., Temu, T. & Cox, J. (2016) The MaxQuant computational platform for mass spectrometry-based shotgun proteomics. *Nature Protocols*, **11**(12), 2301–2319.
- Vartapetian, A.B., Tuzhikov, A.I., Chichkova, N.V., Taliansky, M. & Wolpert, T.J. (2011) A plant alternative to animal caspases: subtilisin-like proteases. *Cell Death and Differentiation*, **18**(8), 1289–1297.
- Vasse, J., Frey, P. & Trigalet, A. (1995) Microscopic studies of intercellular infection and protoxylem invasion of tomato roots by *Pseudomonas solanacearum*. *Molecular Plant-Microbe Interactions*, **8**, 241–251.
- Vera, P. & Conejero, V. (1988) Pathogenesis-related proteins of tomato: p-69 as an alkaline endoproteinase. *Plant Physiology*, **87**(1), 58–63.
- Vera, P. & Conejero, V. (1989) The induction and accumulation of the pathogenesis-related P69 proteinase in tomato during citrus exocortis viroid infection and in response to chemical treatments. *Physiological and Molecular Plant Pathology*, **34**(4), 323–334.
- Vera, P., Yago, J.H. & Conejero, V. (1989) Immunogold localization of the citrus exocortis viroid-induced pathogenesis-related proteinase p69 in tomato leaves. *Plant Physiology*, **91**(1), 119–123.
- Vey, M., Schafer, W., Berghofer, S., Klenk, H.D. & Garten, W. (1994) Maturation of the trans-Golgi network protease furin: compartmentalization of propeptide removal, substrate cleavage, and COOH-terminal truncation. *The Journal of Cell Biology*, **127**(6 Pt 2), 1829–1842.
- Wang, S., Xing, R., Wang, Y., Shu, H., Fu, S., Huang, J. *et al.* (2021) Cleavage of a pathogen apoplastic protein by plant subtilases activates host immunity. *The New Phytologist*, **229**(6), 3424–3439.
- Xiao, Y., Hsiao, T.H., Suresh, U., Chen, H.I., Wu, X., Wolf, S.E. *et al.* (2014) A novel significance score for gene selection and ranking. *Bioinformatics*, **30**(6), 801–807.
- Yu, S.H., Ferretti, D., Schessner, J.P., Rudolph, J.D., Borner, G.H.H. & Cox, J. (2020) Expanding the Perseus software for omics data analysis with custom plugins. *Current Protocols in Bioinformatics*, **71**(1), e105.
- Zuluaga, A.P., Sole, M., Lu, H., Gongora-Castillo, E., Vaillancourt, B., Coll, N. *et al.* (2015) Transcriptome responses to *Ralstonia solanacearum* infection in the roots of the wild potato *Solanum commersonii*. *BMC Genomics*, **16**, 246.
- Zuluaga, A.P., Vega-Arrequin, J.C., Fei, Z., Matas, A.J., Patev, S., Fry, W.E. *et al.* (2016) Analysis of the tomato leaf transcriptome during successive hemibiotrophic stages of a compatible interaction with the oomycete pathogen *Phytophthora infestans*. *Molecular Plant Pathology*, **17**(1), 42–54.